Biochimica et Biophysica Acta 1864 (2016) 655–666

Contents lists available at ScienceDirect

Biochimica et Biophysica Acta

journal homepage: www.elsevier.com/locate/bbapap

The role of the C-terminal region on the oligomeric state and enzymatic activity of *Trypanosoma cruzi* hypoxanthine phosphoribosyl transferase

Wanda M. Valsecchi [a], Alexandra Cousido-Siah [b], Lucas A. Defelipe [c], André Mitschler [b], Alberto Podjarny [b], Javier Santos [a,*], José M. Delfino [a,*]

[a] Instituto de Química y Fisicoquímica Biológicas, Universidad de Buenos Aires, Junín 956, C1113AAD Buenos Aires, Argentina
[b] Department of Integrative Biology, IGBMC, CNRS, INSERM, Université de Strasbourg, Illkirch, France
[c] Departamento de Química Biológica, Facultad de Ciencias Exactas y Naturales and IQUIBICEN-CONICET, Universidad de Buenos Aires, C1428EGA Buenos Aires, Argentina

ARTICLE INFO

Article history:
Received 19 November 2015
Received in revised form 25 February 2016
Accepted 8 March 2016
Available online 10 March 2016

Keywords:
Quaternary structure
Enzymatic activity modulation
Stability
Proteolysis
Reversible oligomerization
Disorder C-terminal region
Bisphosphonates

ABSTRACT

Hypoxanthine phosphoribosyl transferase from *Trypanosoma cruzi* (TcHPRT) is a critical enzyme for the survival of the parasite. This work demonstrates that the full-length form in solution adopts a stable and enzymatically active tetrameric form, exhibiting large inter-subunit surfaces. Although this protein irreversibly aggregates during unfolding, oligomerization is reversible and can be modulated by low concentrations of urea. When the C-terminal region, which is predicted as a disordered stretch, is excised by proteolysis, TcHPRT adopts a dimeric state, suggesting that the C-terminal region acts as a main guide for the quaternary arrangement. These results are in agreement with X-ray crystallographic data presented in this work. On the other hand, the C-terminal region exhibits a modulatory role on the enzyme, as attested by the enhanced activity observed for the dimeric form. Bisphosphonates act as substrate-mimetics, uncovering long-range communications among the active sites. All in all, this work contributes to establish new ways applicable to the design of novel inhibitors that could eventually result in new drugs against parasitic diseases.

1. Introduction

Trypanosomes use the enzyme hypoxanthine phosphoribosyl transferase (HPRT) and hypoxanthine or guanine bases as the substrates to produce IMP or GMP, respectively. *Trypanosoma cruzi* HPRT (TcHPRT) catalyzes the transfer of a mono phosphorylated ribose from phosphoribosyl pyrophosphate (PRPP) to the purine ring. Research has shown that the metabolism of the protozoan parasite *Trypanosoma cruzi* (*T. cruzi*) depends on the salvage of exogenous purines for nucleotide synthesis [1]. In this context, TcHPRT plays a key role in the survival of trypanosomes in their hosts. Therefore, TcHPRT has been identified as a potential target enzyme to design specific inhibitors potentially useful for the treatment of the diseases caused by the protozoan parasite [2,3]. On the other hand, in humans purine nucleotides are synthesized de novo and also salvaged from recycled purine bases and nucleosides. Partial deficiency of human HPRT can result in severe forms of gout, whereas the absence of HPRT activity causes the neurological and behavioral condition known as Lesch–Nyhan syndrome [4–8].

Several high-resolution X-ray crystal structures of this enzyme of *T. cruzi* have been already reported [9–14]. These structures reveal the presence of intermolecular contacts that form large interaction surfaces among subunits more likely stabilizing the quaternary assembly of the protein found in solution. Interestingly, the C-terminus of TcHPRT is ~23 amino acid residues longer than in other known HPRTs (Fig. 1). In addition, this stretch of the protein seems to be poorly structured, as judged by the low electronic density revealed for this region. Nevertheless, at least in one case the coordinates corresponding to the C-terminal extension appear well-defined [14]. Interestingly, the C-terminal region of HPRT can be removed without consequence for structure or for the capability of the enzyme to interact with the affinity resin GMP-agarose, bearing the immobilized reaction product GMP. In fact, proteolysed HPRT yields monoclinic crystals that diffract X-rays to higher resolution (1.4 Å) than the original trigonal crystal form [13].

Although the enzyme TcHPRT was originally identified as a monomer/dimer based on SEC-FPLC experiment results [15], it was described that some homologous enzymes form tetramers in solution, among

Abbreviations: CD, circular dichroism; DLS, dynamic light scattering; DTT, dithiothreitol; ESI-MS, electrospray ionization mass spectrometry; GMP, guanosine monophosphate; HPRT, hypoxanthine phosphoribosyl transferase; Hx, hypoxanthine; IMP, inosine; MALS, multi-angle light scattering; NAYA, N-acetyltyrosinamide; NTA, nitrile tri acetic; PDB, Protein Data Bank; PRPP, 5-phospho-α-D-ribosyl 1-pyrophosphate; PPi, diphosphoric acid; RMSD, root-mean-square deviation; SDS-PAGE, sodium dodecyl sulfate polyacrylamide gel electrophoresis; SEC-FPLC, Size-Exclusion-Fast-Protein-Liquid-Chromatography; TcHPRT, hypoxanthine phosphoribosyl transferase variant from *Trypanosoma cruzi*; $TcHPRT_{H6}$, the same variant as before but carrying the His-tag at the C-terminal end.

* Corresponding authors.
E-mail addresses: javiersantosw@gmail.com (J. Santos), delfino@qb.ffyb.uba.ar (J.M. Delfino).

http://dx.doi.org/10.1016/j.bbapap.2016.03.005
1570-9639/

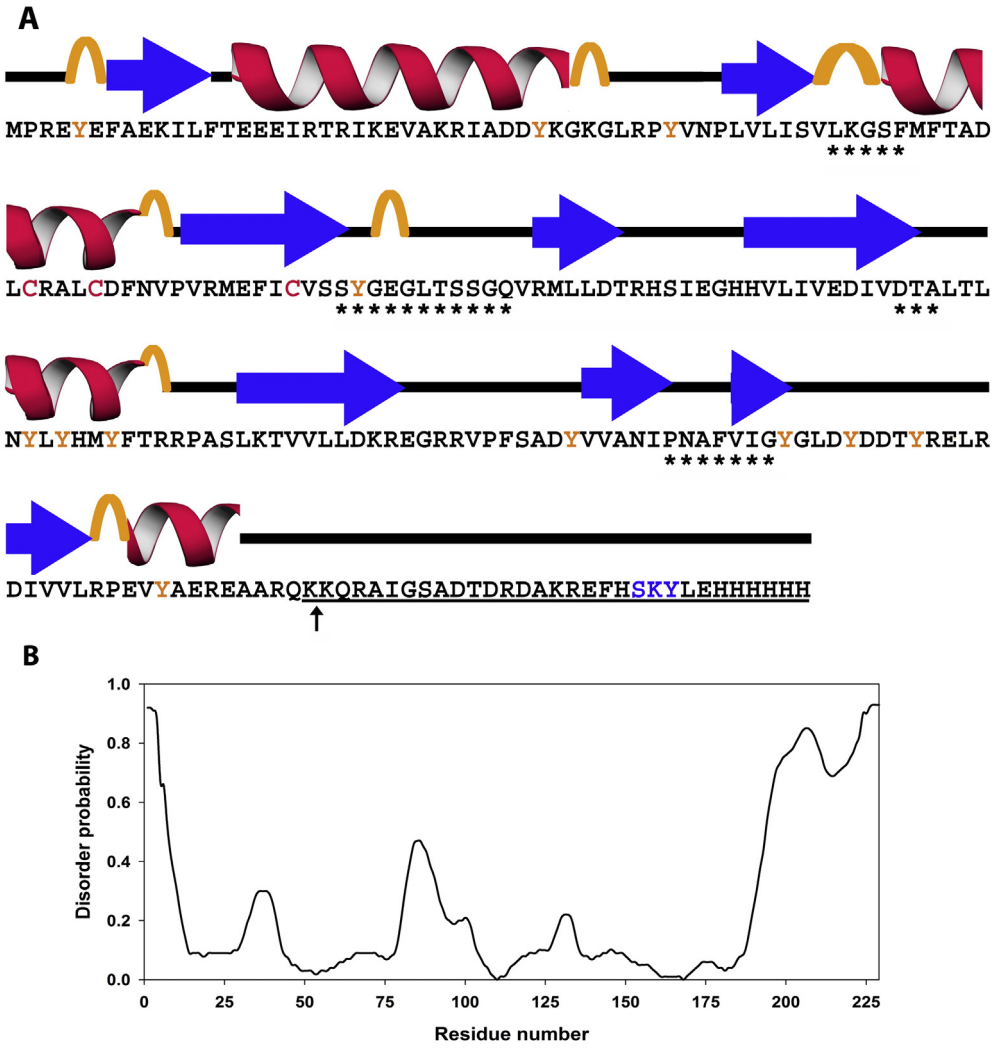

Fig. 1. Primary and secondary structure of $TcHPRT_{H6}$. Secondary structural elements were derived from the crystallographic structure PDB ID: 5EUC. The C-terminal region is underlined and the glycosomal import signal sequence is shown in blue. Tyrosine and cysteine residues are shown in orange and red, respectively. Stars indicate residues of the active site. A profile showing regions with high disorder (calculated using PrDOS [36]) is included below. Other algorithms were also used to predict disorder: among them DisEMBLE [37], POODLE [38], Disprot [39] and IUPred [40]. In all cases, closely similar results were obtained. For simplicity, only the prediction by PrDOS is shown. Taking or not into account the stretch *LEHHHHHH* in the calculations makes scant difference as regards the disorder probability profile of the rest of the protein, i.e. the point in the sequence beyond which disorder takes over remains essentially the same. In fact, variations in this position among the different algorithms are larger than those encountered for a given algorithm with or without the added stretch.

them that from *Toxoplasma gondii* [16] and hypoxanthine guanine phosphoribosyl transferase from *Plasmodium falciparum* (PfHGPRT) [17]. On the other hand, in other organisms like *Leishmania tarentolae*, HGPRT forms a dimer [18,19]. In addition, the orientation of the C-terminal stretches in the TcHPRT structure (PDB ID 1P17, chains B and C, [14]) suggests that a tetrameric structure might be stabilized by inter-subunit interactions involving residues belonging to the C-terminal region.

In this context, we wondered about the oligomeric arrangement adopted by TcHPRT in crystals and in solution, its conformational stability and susceptibility to proteolysis and the relevance for enzymatic activity of quaternary structure. Answering these questions may pave the way for new strategies applicable to rational inhibitor design.

2. Materials and methods

2.1. Protein expression and purification

The coding sequence corresponding to TcHPRT was amplified by PCR from cDNA kindly provided by Dr. S.P. Craig III, following two designs. In one of them, primer HPRTFw of sequence AACTTTAAGAAGGA GATATACATATGCCACGGGAGTACGAGTTTGCAG and primer HPRTRev of sequence GGTGCTCGAGTCAGTACTTGCTATGAAACTC were used to obtain the sequence of the wild type protein under the control of the T7 promoter. In the second instance, primer TcHPRTRev of sequence GGTGCTCGAGGTACTTGCTATGAAACTC was used to obtain a tagged variant (with six His residues) at the C-terminal region. In addition, primers Fw and Rev were designed to contain XhoI and XbaI restriction sites, respectively. PCR products (~670 bp) were purified from agarose gel electrophoresis and ligated into pGEM-T plasmid. The plasmids obtained were digested using both restriction enzymes and the excised fragments were ligated into the pET-22b plasmid. As a verification control, DNA was sequenced. Proteins were expressed in *Escherichia coli* BL21 (DE3) cells using LB containing 50 mg mL^{-1} ampicillin. When OD_{600} reached a value of 0.8–1.0 the expression of TcHPRT was induced (with 1 mM IPTG for 4 h, at 280 rpm and 37 °C). Cells were harvested by centrifugation (at 5000 rpm for 20 min at 4 °C) and stored at −20 °C until use. Typically, 3 g of cells were disrupted by sonication (in a water-ice bath) in 20 mM Tris–HCl buffer, 100 mM NaCl, pH 8. Soluble and insoluble fractions were analyzed by SDS-PAGE. $TcHPRT_{H6}$ was purified from the supernatant by Ni^{2+}-NTA-agarose chromatography using imidazole for the elution. After that, $TcHPRT_{H6}$ was extensively dialyzed against 20 mM Tris–HCl buffer, 100 mM NaCl, pH 8, to remove imidazole. On the other hand, TcHPRT (the protein without tag) was

purified in three steps. First by passage through an ion-exchange chromatography column (cellulose DE52). The protein of interest – collected in the pass-through fraction – was precipitated by the addition of 70% ammonium sulfate and resuspended by dialysis in 20 mM Tris–HCl buffer, 100 mM NaCl, pH 8. Finally, a size exclusion chromatography step in Sephadex G100 was carried out. Purity of the proteins was ascertained by SDS-PAGE. On the other hand, the integrity of the proteins was corroborated by ESI-MS and MALDI-TOF at the local mass-spectrometry facility (LANAIS PROEM, UBA-CONICET). After these protocols, TcHPRT and $TcHPRT_{H6}$ were >95% pure and DNA free.

2.2. Crystallization, data collection, and structure determination

$TcHPRT_{H6}$ was concentrated to 5 mg mL^{-1} and crystallized in 0.1 M MES buffer, pH 6.5 and 12% (*w*/*v*) PEG 20000 at 20 °C. Crystals were cryoprotected in two steps, with the reservoir solution containing 15 and 30% ethylene glycol and flash-cooled in liquid nitrogen. X-ray diffraction data were collected up to 2.65 Å resolution on a X06DA beamline at Swiss Light Source (SLS), in Switzerland. The diffraction data were processed using HKL2000 suite of programs. The crystal structures were solved by molecular replacement using PHASER provided in the CCP4 package [20], based on the PDB structure 1TC2. The dimeric form without extra truncations was used as the starting model. The model was built using COOT [21] and refined using Refmac [22].

2.3. Enzyme-activity assays

The enzymatic activity of TcHPRT and $TcHPRT_{H6}$ was assessed by a spectrophotometric assay, and monitored by the increase in the absorbance at 245 nm corresponding to the appearance of the newly synthesized nucleotide. The assay was performed at 25 °C in 10 mM HEPES buffer, 12 mM $MgCl_2$, pH 7.4. Assays were carried out by varying the concentration of one substrate: hypoxanthine (Hx) from 0 to 100 μM, or phosphoribosyl pyrophosphate (PRPP) from 0 to 250 μM, whereas the concentration of the other substrate was fixed at a saturating concentration (Hx and PRPP, at 50 and 200 μM, respectively). The initial reaction rate (V_0) at each substrate condition was determined by calculating the initial slope of the (quasi) linear change in the absorbance as a function of time, occurring along the first few seconds of each time trace. Fitting of Eq. (1) (corresponding to an ordered bi-substrate system) to the data allowed us to obtain the best parameters describing the enzymatic reaction.

$$\frac{V_0}{V_{max}} = \frac{[PRPP][Hx]}{(Km_{PRPP}Km_{Hx} + Km_{Hx}[PRPP] + [PRPP][Hx])} \quad (1)$$

2.4. Tyrosine fluorescence spectroscopy

Fluorescence emission spectra were recorded in an AMINCO-Bowman Series 2 (AB2) spectrofluorometer. In the range 280–450 nm using an excitation wavelength of 275 nm and a 0.3 cm path length quartz cell. The spectral slit-width was set to 4 nm for both monochromators. After acquisition, each spectrum was corrected by blank subtraction. All spectra were acquired at 25 °C.

2.5. Circular dichroism (CD) spectroscopy

Spectra were acquired in a Jasco 810 spectropolarimeter equipped with a Peltier accessory for temperature control. Protein samples were prepared to a final concentration of 10 and 25 μM for far-UV and near-UV regions, respectively. Circular dichroism (CD) spectra were recorded in the range 190–260 nm (using a 0.1 cm path-length cell) and 240–340 nm (using 0.5 cm or 1 cm path-length cells). Data acquisition was carried out at 25 °C. At least five spectra were acquired at a scan speed of 20 nm min^{-1} and a time constant set at 1 s, and averaged. Finally, a scan of a buffer was properly smoothed and subtracted from each averaged spectrum. Molar ellipticity (deg cm^2 $dmol^{-1}$) was calculated and informed.

2.6. Second-derivative UV-absorption spectroscopy

To perform a second-derivative analysis of the UV-absorption spectra, at least 10 scans were recorded at intervals of 0.1 nm in the range 240–340 nm and at a scan speed of 20 nm min^{-1} using a Jasco V-550 UV–visible spectrophotometer equipped with a Peltier device equilibrated at 25 °C. Protein samples were prepared at 10.0 μM final concentration. In addition, a solution of n-acetyl tyrosine amide (NAYA) was prepared and used as a reference control of the amino acid Tyr in a solvated environment. A scan corresponding to the buffer was acquired under the same conditions, smoothed and subtracted from the averaged spectrum of each protein sample. An ad-hoc Excel® spreadsheet was used to transform the raw numerical data to the corresponding second-derivative spectra.

2.7. Hydrodynamic behavior

Size-exclusion chromatography (SEC) was performed in a FPLC system equipped with UV-detector (Jasco UV2075 plus), multi-angle light scattering (MALS) and dynamic light scattering (DLS) modules (Wyatt Technology). SEC experiments were carried out using a Superose 12 column (General Electric) equilibrated at room temperature. The flow rate was set to 0.3 mL min^{-1} and the injection volume was 100 μL. Protein samples were prepared in the same elution buffer and centrifuged (15,000 rpm at 4 °C) before injection. Data processing was performed using the ASTRA software.

2.8. Protein unfolding followed by CD and fluorescence emission

For denaturant-induced unfolding experiments, proteins were incubated for 4 h in urea solutions at concentrations in the range 0 to 8 M. Unfolding was followed by the change in the intensity of Tyr fluorescence, as described above. On the other hand, thermal denaturation of TcHPRT and $TcHPRT_{H6}$ variants was monitored in a Jasco 810 spectropolarimeter by the change in the CD signal at 220 nm with temperature (in the range 0 to 100 °C, at a ramp rate of 1 °C min^{-1}). To evaluate the reversibility of the unfolding reaction and the eventual appearance of aggregates, protein samples were incubated in 3, 6 and 8 M urea and subsequently dialyzed to eliminate the denaturant. UV-absorption and fluorescence spectra were acquired before and after dialysis. Prior to measuring fluorescence or absorption, samples were centrifuged at 15,000 rpm for 20 min to eliminate possible misfolded protein aggregates.

3. Results

3.1. The conformation of TcHPRT in solution

TcHPRT was efficiently expressed in *E. coli* cells and purified from the soluble fraction. Two variants were prepared, $TcHPRT_{H6}$ and TcHPRT, the enzyme forms with or without a tag of six His residues (His-tag) located at the C-terminus of the protein to facilitate purification. First of all, we compared the spectroscopic properties of both variants. Far-UV CD spectra (Fig. 2A) indicate that both variants exhibit similar secondary structure content. In addition, no differences are observed when the second-derivative of the UV absorption spectra corresponding to the two variants are compared, i.e. the same components with no shift in wavelength are observed, suggesting similar structures (Fig. 2C). Small differences in the aromatic environment of Tyr residues can be inferred from the near-UV CD (Fig. 2B). These changes can be tentatively attributed to a shift in the protonation state of phenolic side chains.

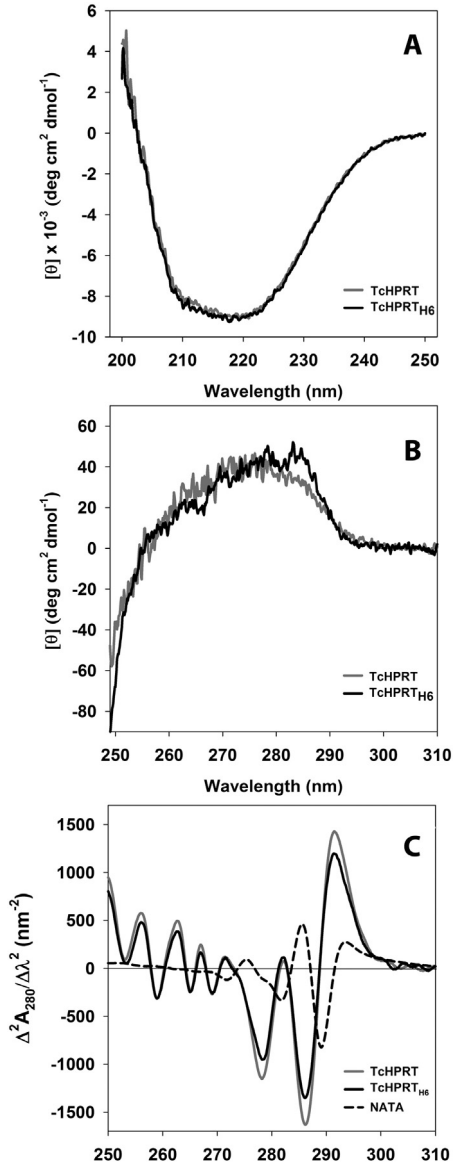

Fig. 2. Spectroscopic characterization of TcHPRT. Far-UV CD (A), near-UV CD (B) and, second derivative absorption UV spectra (C) corresponding to the full-length and His-tagged variants are shown. For comparison, the spectrum of N-acetyl tyrosinamide (NAYA) is also shown in panel C. Protein concentration is 15, 45, and 30 μM, in A, B and C, respectively, in 20 mM Tris–HCl buffer, 100 mM NaCl, pH 8.0. Experiments were carried out at 20 °C. The far-UV CD data, extended to 187.8 nm, were submitted for analysis in the server [41]. After fulfilling the appropriate statistical criteria, the algorithm SELCON3, with Datasets 4 or 7, produced the following % values: 10% helix1, 8% helix2, 19% strand1, 12% strand2, 22% turns, 29% unordered. These numbers agree reasonably well with the secondary structure content derived from PDB ID 5EUC, using the DSSP program according to Kabsch and Sander criteria [42]: 27% helix, 25% strand.

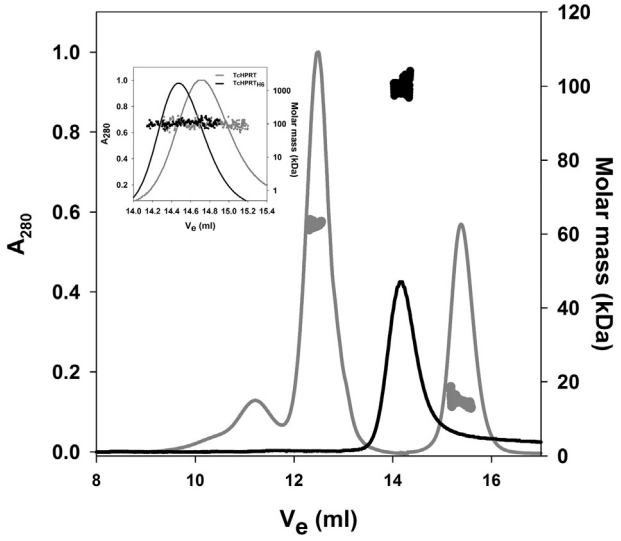

Fig. 3. Hydrodynamic behavior of TcHPRT variants (SEC-FPLC in Superdex S200, black trace). Protein concentration is 55 μM in 20 mM Tris–HCl buffer, 100 mM NaCl, pH 8.0. The experiments were carried out at room temperature. As a reference, two globular proteins were assayed under identical conditions (trace in gray): bovine serum albumin (BSA, 66 kDa) and *human* frataxin (FXN, 14 kDa). The molar mass was determined using a MALS detector in line with the UV detector and ASTRA software. The inset shows a detailed view of the elution profile corresponding to full-length and His-tagged TcHPRT variants.

On the other hand, to evaluate the quaternary structure in solution of both $TcHPRT_{H6}$ and TcHPRT variants, light-scattering experiments were performed in a series of buffer conditions. Our results show that the protein behaves mostly as a tetramer (~100 kDa) in a broad range of protein concentrations and buffer conditions (Figs. 3 and S1). ESI-MS and SDS-PAGE evidence indicates the prevalence of a monomeric entity, thus pointing to the fact that the tetrameric structure is stabilized by non-covalent interactions. Nevertheless, in the absence of the reducing agent DTT a minor fraction of the molecules (less than 5%) becomes covalently linked through intermolecular disulfide bonds (data not shown). Interestingly, the elution volume of the protein after size-exclusion chromatography is definitely anomalous. Thus, regardless of the presence or absence of the His-tag, the TcHPRT tetramer (~100 kDa) elutes after the BSA marker (~66 kDa) (Figs. 3 and S1B). Moreover, increasing NaCl concentration partially reverses this effect, a behavior that is well documented for proteins that exhibit some kind of interaction with the chromatographic matrix. Positively charged proteins usually interact favorably with the matrix, whereas negatively charged ones are excluded by charge repulsion. Moreover, apolar interactions may also take place between matrix and proteins, producing atypical behaviors [23–25].

In addition, to explore the stability of the variants, urea-induced and temperature unfolding experiments were carried out (Figs. 4, S2 and S3). Urea-induced unfolding followed by the change in Tyr fluorescence presents some complexity, because at least two transitions are observed. The first one occurs in the range 0–2 M urea and the second one happens between 2 and 4 M. However, protein aggregation taking place after dialysis or denaturant dilution, an indication of the existence of an irreversible phenomenon, precludes the derivation of thermodynamic state functions from the unfolding data. Nevertheless, both variants seem to behave as cooperative folding units when submitted to chemical or thermal denaturation. In particular, a qualitative comparison (a shift in the observed apparent T_m values) of thermal denaturation curves suggests that the His-tag present in $TcHPRT_{H6}$ might enhance its thermostability by increasing the height of the activation barrier to the formation of aggregation-prone species. Nevertheless, when each variant is incubated for 10 min at 60 °C, they irreversibly aggregate with a concomitant loss of enzymatic activity (Fig. S4). Alongside the first urea-induced transition followed by fluorescence, incubation of each variant with low denaturant concentrations (in the range 1–2 M urea) perturbs the quaternary structure of the macromolecules, promoting the disassembly of the tetramer into dimeric and monomeric forms (Fig. 5). It is worthy of note that this process proves to be reversible, as judged by SEC-FPLC and light scattering: dialysis of urea promotes the reassembly of the quaternary structure of both variants TcHPRT and $TcHPRT_{H6}$. These results suggest that the aggregation-prone states take place along monomer refolding (or unfolding), but not along subunit association or dissociation of the tetramer.

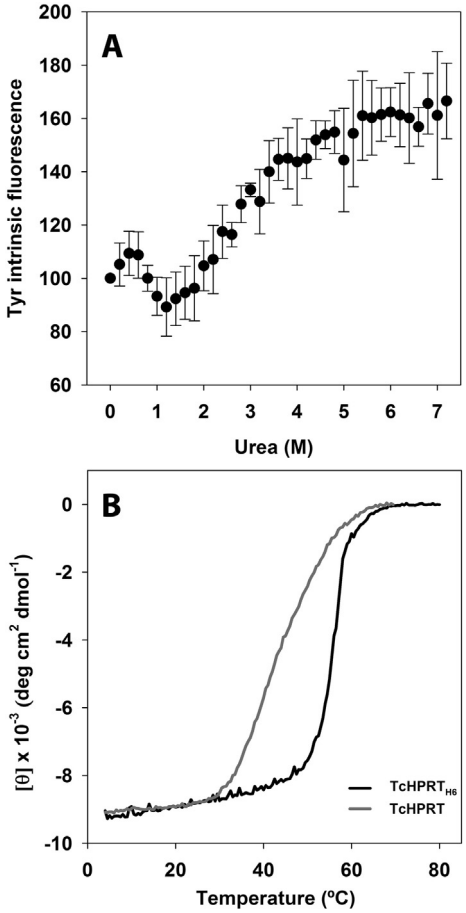

Fig. 4. TcHPRT denaturation experiments. (A) Urea-induced unfolding of His-tagged TcHPRT followed by tyrosine fluorescence intensity. Experiments were carried out at 20 °C. (B) Thermal denaturation profiles corresponding to full-length and His-tagged TcHPRT variants in 20 mM sodium phosphate buffer, 100 mM NaCl, pH 8.0.

3.2. The C-terminal stretch of TcHPRT is essential to attain the tetrameric arrangement of the protein

Next, we decided to investigate whether the oligomeric arrangement of TcHPRT may be subject to intervention by challenging the protein with proteases. If TcHPRT is incubated with trypsin, the protein is rapidly digested to a shorter form and subsequently degraded into small peptide fragments, as judged by SDS–PAGE analysis of the reaction mixture (Fig. 6). At very short times of digestion we managed to isolate a major product of digestion by SEC-FPLC on a Superose 12 column and found that the first cut corresponds to the excision of the stretch of residues that is predicted to form the mobile C-terminal segment. The site of cut, as confirmed by MALDI and ESI–MS, is marked with a black arrow in Fig. 1. Once shortened, the quaternary structure of TcHPRT by SEC-FPLC and light scattering reveals that the protein behaves as a dimer in solution. This result firmly suggests that the C-terminal stretch, even though predicted as a highly disordered segment, stabilizes the tetrameric conformation of TcHPRT. Far-UV CD spectra and temperature unfolding experiments were carried out to evaluate whether the dimer is well folded (Fig. 7). These results confirm that the conformation remains intact after the C-terminal split. As in the case of the tetramer, dimeric TcHPRT aggregates irreversibly upon thermal denaturation, a fact that makes impossible any thermodynamic analysis aimed at extracting meaningful free energy data. Nevertheless, the observed T_m for the denaturation transition of the fragment suggests a thermal stability similar to the full-length protein.

3.3. Truncation of the C-terminal stretch of TcHPRT$_{H6}$ enhances its catalytic efficiency

Enzymatic activity is exquisitely sensitive to fine perturbations of the protein structure. Therefore, we decided to evaluate the effect of controlled proteolysis on TcHPRT$_{H6}$ activity using trypsin as a probe. After incubation with this protease at high dilution, the reaction was stopped at defined periods by the addition of a Ser protease inhibitor (1 mM PMSF) and the protein sample was loaded onto an analytical SEC-FPLC column (Superose 12, Fig. 6). HPRT activity was assayed for fractions containing the shorter variant. As a control, the enzymatic activity of the untreated enzyme was assayed under the same experimental conditions. Despite the C-terminal truncation, results indicate that this short form would exhibit an enhanced enzymatic activity (Fig. 8A), a fact indicative of a subtle perturbation of the active site region. Importantly, the variant of the enzyme *without* the His-tag (TcHPRT) exhibits *lower* activity than the C-terminal truncated variant (Fig. 8A). Indeed, the slight decrease in the activity of TcHPRT as compared to that observed for TcHPRT$_{H6}$ can be attributed to a minor positive modulating effect due to the presence of the stretch *LEHHHHHH* in the latter variant.

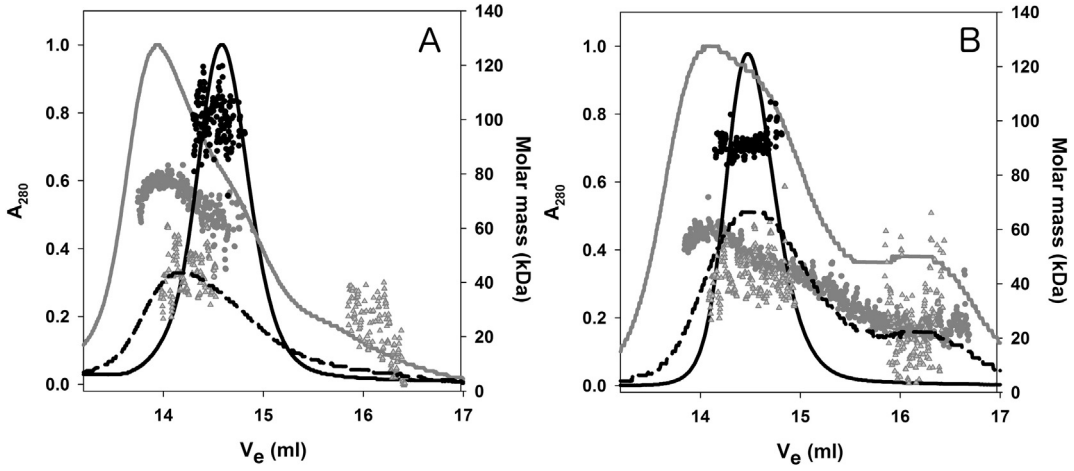

Fig. 5. Tetramer reassembly equilibrium experiment. SEC-FPLC experiments were carried out in a Superdex S200 column and a MALS detector in line with the UV detector. Molar mass was analyzed using ASTRA software. TcHPRT (A) and TcHPRT$_{H6}$ (B) protein samples (at low and high concentrations, in dashed black and continuous gray lines, respectively) and column were equilibrated at 20 °C in 1 M urea dissolved in 20 mM Tris–HCl buffer, 100 mM NaCl, pH 8.0. After dialysis of urea, the elution profile corresponds to the continuous black line and the molar mass to the black circles.

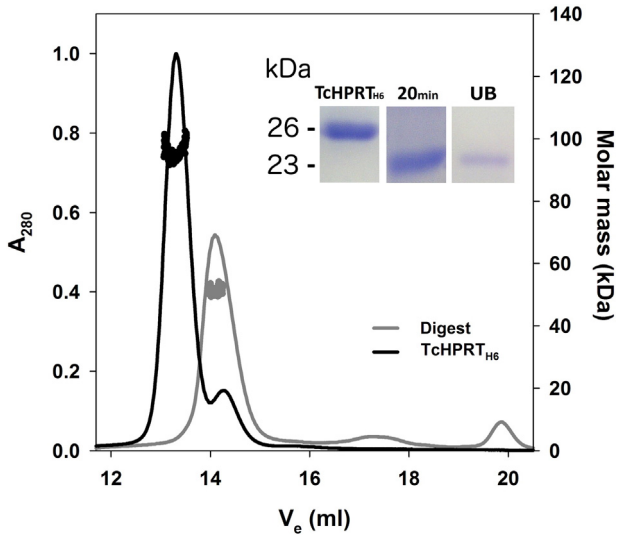

Fig. 6. Hydrodynamic behavior of TcHPRT after the excision of the C-terminal region. TcHPRT$_{H6}$ was loaded onto SEC-FPLC before (black line and circles) or after (gray line and circles) protease treatment for 20 min. Experiments were carried out using a Superdex S200 column and a MALS detector in line with the UV detector. Molar mass was analyzed using ASTRA software. Inset: The same samples were loaded onto SDS-PAGE. In addition, protein was loaded onto a NTA-agarose column and the unbound fraction was run side by side (UB).

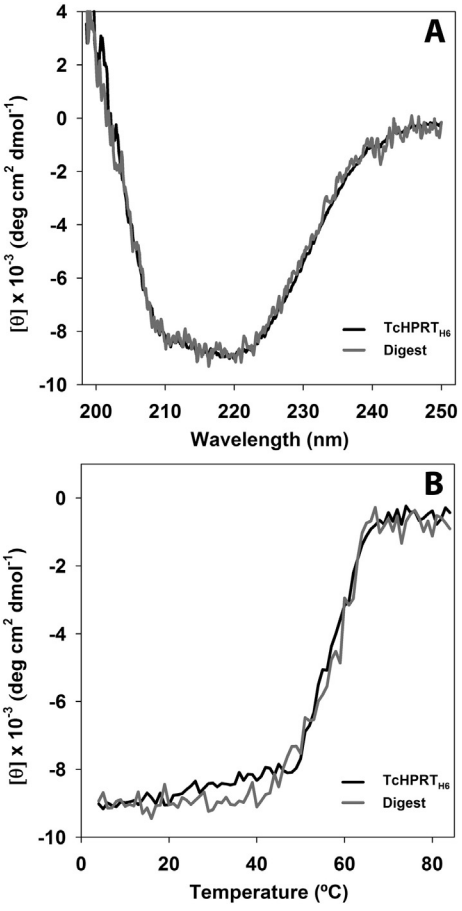

Fig. 7. Analysis of the conformation of the purified TcHPRT dimer. Far UV CD spectra (A) at 20 °C and the thermal denaturation trace (B) are shown, corresponding to the dimeric form of TcHPRT dissolved in 20 mM sodium phosphates buffer, 100 mM NaCl, pH 8.0. As a reference, identical experiments with the tetrameric form are shown side by side.

To validate this observation, we decided to explore this activation phenomenon in real time, that is, by monitoring HPRT enzymatic activity along the course of proteolysis, without any separation of molecular species (Fig. 8B). At short incubation times, an increment in the catalytic efficiency occurs reaching a maximum of ~20% above that observed for the untreated enzyme, whereas at longer incubation times HPRT activity diminishes, most likely as the consequence of further digestion of the protein, a fact confirmed by the appearance of lower molecular weight fragments by SDS-PAGE.

3.4. The tetrameric structure of TcHPRT$_{H6}$ determined by X-ray crystallography and the internal mobility of the protein

Both variants TcHPRT$_{H6}$ and TcHPRT were submitted to crystallization trials, but only the first produced crystals suitable for diffraction. At variance, the latter gave rise to small crystals that did not diffract well, even under synchrotron beam radiation. After having solved the structure of TcHPRT$_{H6}$ by X-ray crystallography (Table 1, PDB ID: 5EUC), we were able to evaluate the interfaces among monomers in the putative tetramer. In agreement with light scattering measurements, TcHPRT$_{H6}$ emerges as a clear-cut tetramer (Fig. 9). Furthermore, analysis of the X-ray data indicates that the TcHPRT$_{H6}$ structure consolidates in a way in which monomers establish two different interfacial contacts, giving rise to two alternative dimeric arrangements (dimer 1 and dimer 2). One of the interfaces is considerable larger than the other (~1700 and ~1000 Å^2 for dimer 1 and 2, respectively) and the latter is presumably stabilized by contacts involving the C-terminal stretch of the protein. Taking into account that controlled tryptic digestion results in dimer formation, one wonders which one (dimer 1 or dimer 2) is the predominant species present in aqueous solution after this treatment. Thus, it seems reasonable that truncation of TcHPRT$_{H6}$ results in dimer 1, ruling out the involvement of the C-terminal stretch in intermolecular interactions. Suggestively, dimer 1 superimposes perfectly with the structure of the TcHPRT dimer observed at high resolution (1.4 Å, PDB ID: 1TC2), in which 22 amino acid residues were removed from the C-terminus of the enzyme [12]. These observations are also in agreement with the expected higher stability conferred by monomer–monomer interactions (calculated using the PISA server, http://www.ebi.ac.uk/pdbe/pisa/) in the case of dimer 1 as compared to dimer 2 (~− 17.0 and − 1.5 kcal mol^{-1}, respectively).

Remarkably, by comparison with previously reported structures of TcHPRT, this new structure does not exhibit significant changes, as judged by the low RMSD (0.15 Å) values observed for each one of the monomeric units in the new crystal structure when compared to PDB ID: 1TC2, one of the available structures of TcHPRT [11]. However, given the low resolution of the present structure (2.65 Å) it is not expected to see major changes in the monomers compared to existing structures. It is worthy of note that the larger differences occur in loop 81–92 (Fig. 10), a functionally relevant element in this protein [26]. Interestingly, the structure 1TC2 shows that loop 81–92 can acquire at least two different conformations. In one of them, the loop turns away, exposing to the solvent a large area of the protein including the active site. By contrast, the second orientation of loop 81–92 gives rise to a closed and much more compact conformation. It was previously suggested that the interchange between both conformations might contribute to TcHPRT activity, providing access to catalytic sites and optimizing binding interactions along the catalytic cycle. At variance with the former, the structure reported in this paper intriguingly shows an intermediate conformation for this relevant loop of the protein (Fig. 10A and B). Altogether these results point to the conformational flexibility of this stretch. In agreement with this picture, loop 81–92 exhibits the highest B-factors of the crystal structure (Fig. 10C), indicating the inherent high mobility of this region. Since this form corresponds to the apo enzyme, the flexible loops involved in substrate binding in the active site are expected to be adopting a multitude of conformations. In addition, loop 52–55 and loop 69–70 exhibit slightly increased

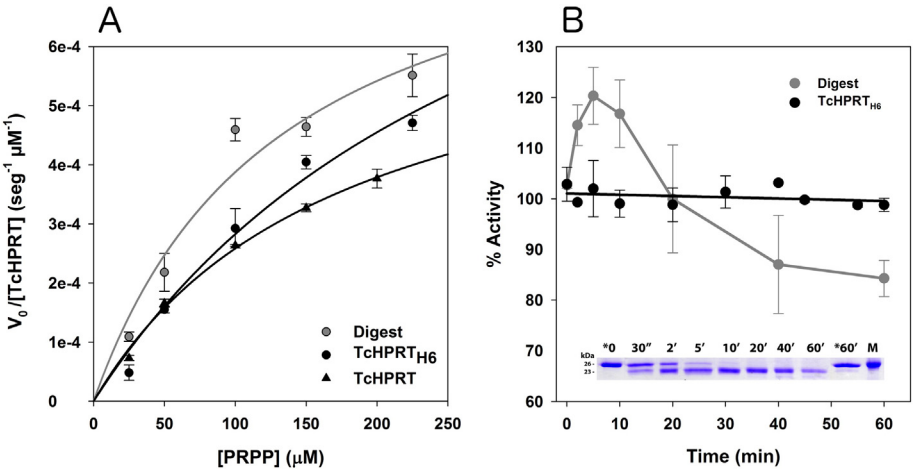

Fig. 8. Enzymatic activity of TcHPRT variants. (A) Comparison of the enzymatic activity of TcHPRT$_{H6}$ and TcHPRT variants (black circles and black triangles, respectively), with proteolytically treated and purified TcHPRT$_{H6}$ (gray circles). The assay includes 10 mM HEPES buffer, 12 mM $MgCl_2$, pH 7.4 with the addition of 50 μM hypoxanthine and variable concentrations of PRPP. Activity was measured at 25 °C as the difference in the absorbance at 245 nm. To normalize the different length of these variants, enzymatic activity is expressed in s^{-1} μM^{-1}. (B) Change in the enzymatic activity of TcHPRT$_{H6}$ along proteolysis. Activity expressed as the percentage (%) of the initial value was evaluated in the presence (gray) or in the absence (black) of protease (1:100 *w/w* protease to TcHPRT$_{H6}$). Enzymatic assay was carried out with 50 μM hypoxanthine and 200 μM PRPP as substrates. The inset shows the profile of the proteolytic reaction by SDS-PAGE. The lane 60* is a control sample of TcHPRT$_{H6}$ incubated for 60 min without protease, and M is a protein marker of 26 kDa.

RMSD values. Remarkably, although the former is also part of the active site, loop 52–55 occupies a location far from it, but is directly connected to β-strand 45–51, whose C-terminal end is in turn connected to loop 52–55.

On the other hand, the C-terminal stretch of each subunit also shows considerably high B-factor values, pointing to the flexibility of this part of the chain. Finally, we were not able to locate the C-terminal residues Q198 to Y221, suggesting that – as it happens in other crystal structures – this tract of the protein is highly flexible and most likely disordered.

One interesting question is why TcHPRT stabilizes as a tetramer in solution, even though the C-terminal region of the protein exhibits an aperiodic structure that may be predicted as a locally disordered segment. Indeed, a structure of HPRT (PDB ID: 1P17, [14]) has been reported suggesting a tetrameric arrangement rather than a dimeric one. It is noteworthy that here the C-terminal regions prolong the protein chains roughly in the same direction dictated by the preceding C-terminal helices, despite the fact that they do not exhibit regular order. Thus, the C-terminal region of a given subunit likely interacts with the N-terminal stretch of the neighboring subunit located diagonally in front of it, establishing a multiplicity of contacts. This fact is illustrated in the case of subunits B and C (Fig. S5). Despite being a highly mobile element, the C-terminal stretch might nevertheless contribute to stabilize the quaternary arrangement. We hypothesize that this highly dynamic segment serves to build a bridge that imparts cohesion to the tetramer. In this fashion, charged residues located in this segment may establish stabilizing electrostatic interactions. Unfortunately, we fail to discern the putative side-chain contacts formed by R211 with E9 belonging to subunit C. In the model, the guanido group of R211 lies at about 3 Å from the carboxyl end of E9.

Table 1
Data collection and refinement statistics of X-ray crystal structure TcHPRT$_{H6}$.

Data collection	
Space group	P 31
Cell dimensions	
a, b, c (Å)	95.66 95.66 75.68
α, β, γ (°)	α = β = 90 γ = 120
Resolution (Å)	50.0–2.65 (2.74–2.65)
R_{sym} (%)	9.5 (45.5)
I/σI	13.6 (3.1)
Completeness (%)	99.9 (99.7)
Redundancy	3.7 (3.7)
Refinement	
Resolution (Å)	36.34–2.65
No. reflections	22,514
R_{work}/R_{free} (%)	17.91/25.35
No. atoms	
Protein	6278
Water	111
rms deviations	
Bond lengths (Å)	0.012
Bond angles (°)	1.540
Ramachandran favored (%)	95.95
Ramachandran outliers (%)	0.65
Ramachandran allowed (%)	3.39
Clashcore	5.32

*Values in parentheses are for the highest-resolution shell.

3.5. Probing the catalytic function of TcHPRT with bisphosphonate inhibitors

Given that some bisphosphonate derivatives have shown substantial inhibitory effect on TcHPRT [27], the active site of the tetrameric protein was probed using the following set of these compounds: alendronate, ibandronate, lidadronate, olpadronate, pamidronate and zoledronate (Fig. 11). Interestingly, two of them – ibandronate and zoledronate – show a clear inhibitory effect (Fig. 11), suggesting that they can act as substrate mimetic in the context of the tetrameric TcHPRT enzyme. Preliminary docking computations suggest that bisphosphonates interact with the protein through their negatively charged region in the same way as PRPP does (through backbone interactions of D115, T116 and A117 and the side chain of T116). Although we observe a spectrum of possible interactions of different amino groups most likely, depending on the length and chemical properties of each chain, the negatively charged region in each of these compounds seems to interact with the same amino acid residues of the protein, reinforcing the notion that bisphosphonate compounds act via binding to the active site (Fig. S6). Current efforts in our laboratory point to obtaining crystals including bisphosphonate inhibitors present in the drops. In particular, even though these inhibitor molecules might exhibit low to moderate affinity, we consider that the study of their detailed interaction with HPRT may help in the design a new generation of inhibitors of higher affinity.

To a larger or lesser extent, all bisphosphonates assayed act on the enzyme by giving rise to an activation effect evident up to 100–150 μM concentration. Beyond this point, the inhibitory effect prevails. Long-range communications among the active sites of different

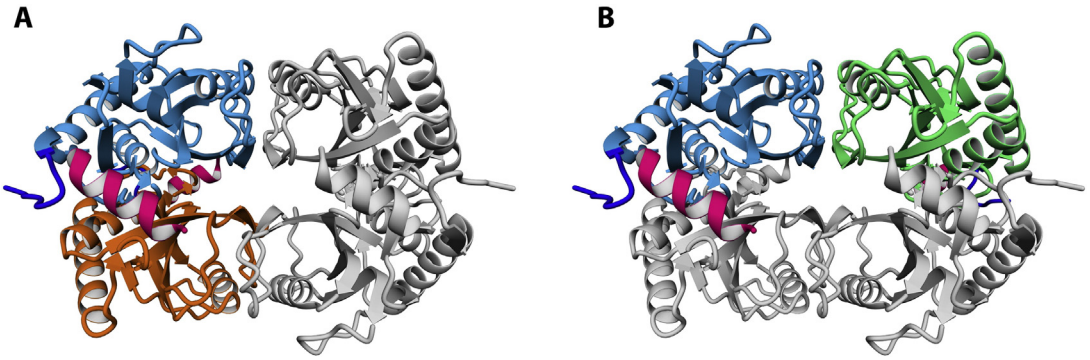

Fig. 9. The X-ray crystal structure of $TcHPRT_{H6}$ reveals two putative dimeric interfaces. Dimers 1 and 2 are highlighted in colors in panels A and B, respectively. Protein structure is represented in ribbon diagrams. The N- and C- terminal stretches are shown in blue and red, respectively.

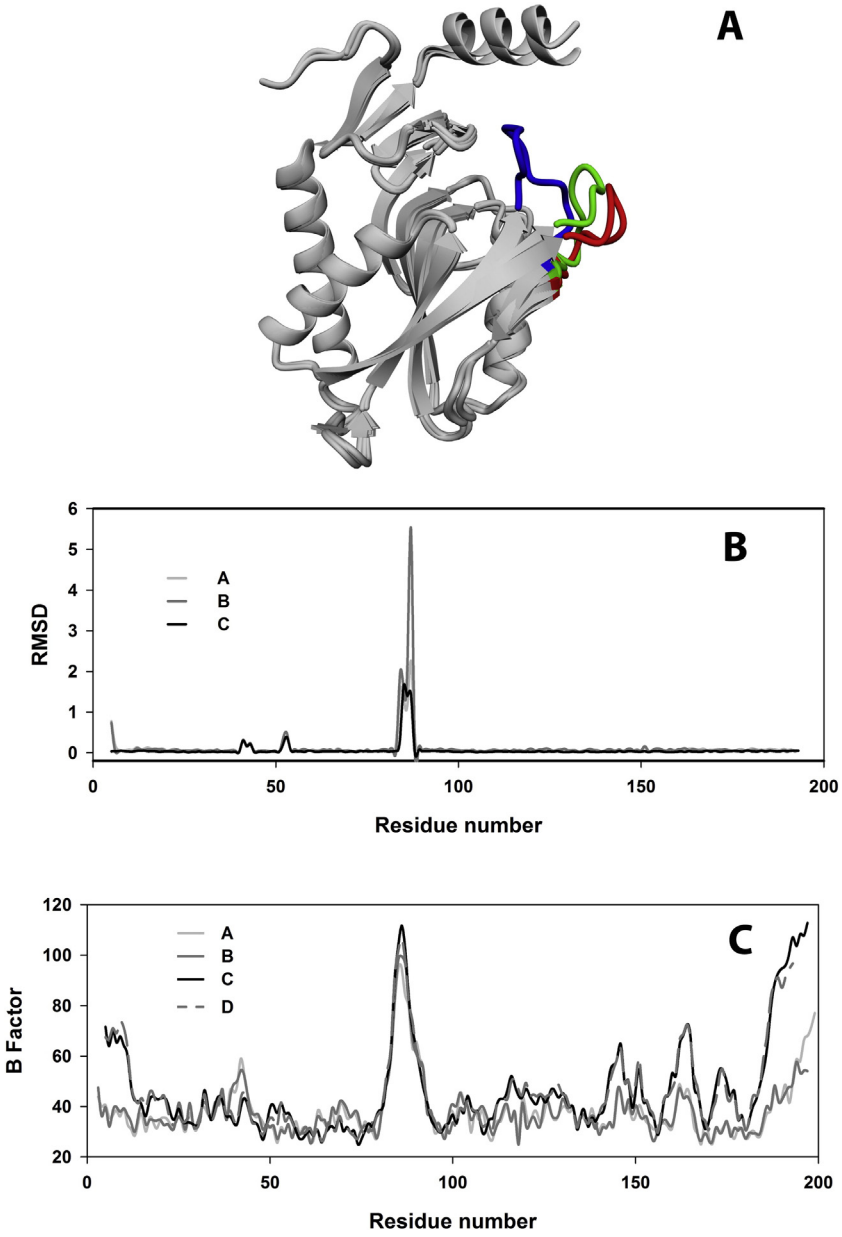

Fig. 10. Analysis of the X-ray crystal structure of $TcHPRT_{H6}$. (A) RMS superimposition of chain A from PDB ID: 5EUC and chains A and B of PDB ID: 1TC2. The open and closed conformations of loop 81–92 are shown in red and blue, respectively. An alternative conformation for this loop is found in the structure solved in the present work (green). (B) The root-mean-square deviations (RMSD) of alpha carbon atoms positions corresponding to each one of the protein chains (A in light gray, B in dark gray, C in black) upon chain D used as the reference are shown. (C) B-factors corresponding to the alpha carbon atoms of each chain: A in light gray, B in dark gray, C in black, and D in dashed dark gray.

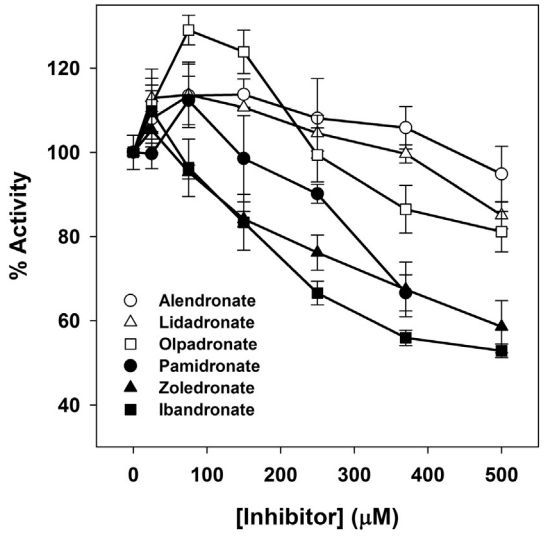

Fig. 11. Inhibition of $TcHPRT_{H6}$ enzymatic activity by bisphosphonates. These compounds (alendronate, lidadronate, olpadronate, pamidronate, zoledronate and ibandronate) were assayed against the tetrameric form of TcHPRT. The assay was performed in 10 mM HEPES buffer, 12 mM $MgCl_2$, pH 7.4 at 25 °C. Hypoxanthine and PRPP concentrations were 25 and 85 μM, respectively. Activity was monitored by the change in absorbance at 245 nm.

subunits, supported by the quaternary arrangement of this protein, most likely underlies this cooperative phenomenon. A detailed study of this biphasic behavior will be the matter of further mechanistic studies on TcHPRT.

Interestingly, the largest inhibitory power is verified in the case of zoledronate, a compound bearing an imidazole ring able to delocalize a positive charge at neutral pH. Likewise, risedronate behaves similarly by virtue of its pyridine ring ([27], see discussion there). An implication of this fact is that, after being locked through the bisphosphonate anchor, a diffuse positive charge strategically located within the active site might resemble the transition state of the pyrophosphorolysis and condensation reaction.

3.6. Discussion

Full-length TcHPRT in solution adopts a stable and enzymatically active tetramer form exhibiting considerably large inter-subunit surfaces. This finding is at odds with a previous interpretation of the enzyme as a monomer/dimer, as suggested by SEC [15] and elaborations on the associations present in the crystallographic structure corresponding to a shorter variant [11]. Moreover, the oligomerization process was found to be reversible and can be modulated by low concentrations of urea (in the range 1–2 M). This perturbing agent shifts the equilibrium, so that the dimeric and monomeric forms become mostly populated in the mixture. Significantly, removal of the denaturant by dialysis promotes the reassembly of the tetramer. At higher urea concentrations, the monomeric form undergoes denaturation, but irreversible aggregation occurs concomitantly, precluding any thermodynamic characterization of the process. When the C-terminal region, which is predicted as disordered, is excised by a gentle protease treatment, $TcHPRT_{H6}$ adopts a dimeric conformation, firmly suggesting that the C-terminal region mediates the interaction between dimers favoring oligomerization. Remarkably, this dimeric form of the molecule exhibits modestly enhanced activity – it is about 20% more active than the tetramer – and keeps similar spectroscopic features, pointing to a preserved overall native conformation. Nevertheless, fine structural readjustments, changes in local dynamics and/or facilitated access to the catalytic site might underlie this activation effect. In any case, to build a full picture of the effects of structural elements on enzymatic activity, one would need a careful evaluation of the cooperative behavior exhibited by substrates and inhibitors (results not shown).

The C-terminal region of TcHPRT not only plays a major role for the integrity of the quaternary structure of the enzyme, but might also bear importance as a key signaling motif for the correct compartmentalization of the protein. In *T. cruzi*, HPRT finds its location in the glycosomal compartment, a process mediated by a C-terminal glycosomal import signal (PTS1) of sequence SKY (residues 219–221). Interestingly, in the case of TcHPRT this signal is located in the 28-residue-long C-terminal stretch predicted as disordered. Remarkably, in the $HPRT_{H6}$ crystal structure, the C-terminal helix extends up to residues 191–195, i.e. the last residue in α-helical conformation of each chain being 195 in chain A, 194 in chains B and C, and 191 in chain D, leaving a disordered stretch of 26–30 residues at the end, thus falling in good agreement with the predictions.

Although HPRTs from other *Trypanosoma* and *Leishmania* parasites also bear C-terminal disordered regions, TcHPRT shows the longest stretch (Fig. S8). Intrinsic disorder may be important for the correct location/translocation of TcHPRT. Whether this is only the consequence of the location of the signal – namely, in general C-terminal stretches are dynamic segments – or if, alternatively, a structural requirement for flexibility exists for a protein–protein interaction relevant for import to the glycosome is an open question. However, in the case of protein import to the peroxisome, Neuberger et al. [28] reanalyzed published data concluding that at least a stretch of 12 C-terminal residues of the target protein are implicated in the recognition process. This motif can be structurally and functionally divided into three regions: (i) the C-terminal tripeptide, (ii) a region comprising four residues further upstream that interacts with the surface of the cytosolic cargo receptor binding proteins, and (iii) a solvent accessible and unstructured linker region. Remarkably, protein unfolding is not a prerequisite for import to glycosomes. One of the first examples showing that folded proteins can be imported into glycosomes was reported for DHFR in *Trypanosoma brucei* [29]. In addition, it was demonstrated that proteins like chloramphenicol acetyl transferase enter as oligomers into peroxisomes in vivo [30]. This evidence points to the possibility that TcHPRT could be imported in the tetrameric conformation. In addition, one may suspect that inside the glycosome, the C-terminal stretch could be excised by proteolysis, giving rise to the dimer. Whether a tetramer or a dimer arising after C-terminal truncation is present inside the glycosome will be the matter of further studies. Perhaps the quaternary structure of this protein might be important to increase the life time of the protein in the cell. This might take place by enhancing the unfolding activation energy barrier, and/or by decreasing the intrinsic tendency of the protein to aggregate (as a consequence of lowering the dimer/monomer concentration. In vivo experiments currently underway will help to clarify this point.

Noteworthy, the X-ray crystal structure of the protein shows that TcHPRT is rather rigid. However, loop 81–92 seems to be one exception to that behavior. Here we show that this loop may acquire conformations alternative to those observed before (open and closed). In a previous work [26] it was shown that the absence of this important loop, which is closer to the active site region, modulates the Michaelis constants (K_m) for substrates slightly (by 0.6–2.7-fold), whereas pyrophosphate exhibits a 5.8-fold increase. By contrast, k_{cat} values are critically affected by loop deletion: the rates are two to three orders of magnitude lower than for the wild-type enzyme. Moreover, it was shown that some residues of this stretch participate directly in the chemistry of the reaction: main-chain nitrogen atoms of residues S81 and Y82 (sequence numbering according to structure PDB ID: 1P17) and the O1A atom of PRPP or PPi, whereas other residues contribute to loop flexibility and folding [31]. The bisphosphonate compounds studied herein exhibit substantial inhibitory activity. In principle, they mimic the PRPP substrate, and at low concentration they may positively modulate the enzymatic activity through the allosteric communication among subunits influencing the catalytic sites. If it were the case, upon binding they might alter the dynamics of loop 81–92. The analysis of B-factor values in co-crystals may contribute to the understanding of this issue.

Remarkably, zoledronate exhibits the largest inhibitory effect of the set of molecules assayed in this work. This ligand is able to delocalize a positive charge in the aromatic imidazole ring at neutral pH. After positioning the bisphosphonate moiety within the active site, the diffuse positive charge in the ring might strategically locate in a position where the transition state of the reaction also develops a positive charge [11]. More importantly, this strategy might be used in the design of a new family of inhibitors. On the other hand, it will be critical to track and de-convolute both the activation and inhibitory effects of these molecules and their effect on the structural dynamics.

Pyrophosphate analogs could be selective for a number of enzymes from parasites. The proton-translocating pyrophosphatase activity is inhibited by imidodiphosphate [32]. In addition, bisphosphonate molecules exhibit an inhibitory effect on farnesyl pyrophosphate synthase from *T. cruzi* [33,34]. In this context, the response observed – the arrest of the proliferation of *T. cruzi* in an in vivo assay [35] – is the consequence of a multi-target effect (most likely including HPRT) of these compounds.

Regarding the relevance of the quaternary arrangement, it is important to notice that the human variant of HPRT also forms a tetramer in solution, albeit of a different nature. Most relevantly for drug design, the human form is inhibited to a *much lesser extent* by the set of bisphosphonates assayed here (results not shown). Indeed, here the entire disordered C-terminal region present in the *T. cruzi* enzyme is absent in the human protein (Fig. 12). In this context, one wonders how the interaction between protomers occurs in the context of the human oligomer. The analysis of the X-ray structure of the human HPRT shows that, even though the protein forms a tetramer constituted of very similar protomers, their relative orientation is quite different, giving rise to an arrangement non-superimposable with that of the TcHPRT variant (Fig. 12). Remarkably, the C-terminal ends in the TcHPRT set point inwards, giving rise to the cross interaction described above, whereas they are oriented outwards in the human enzyme. Conversely,

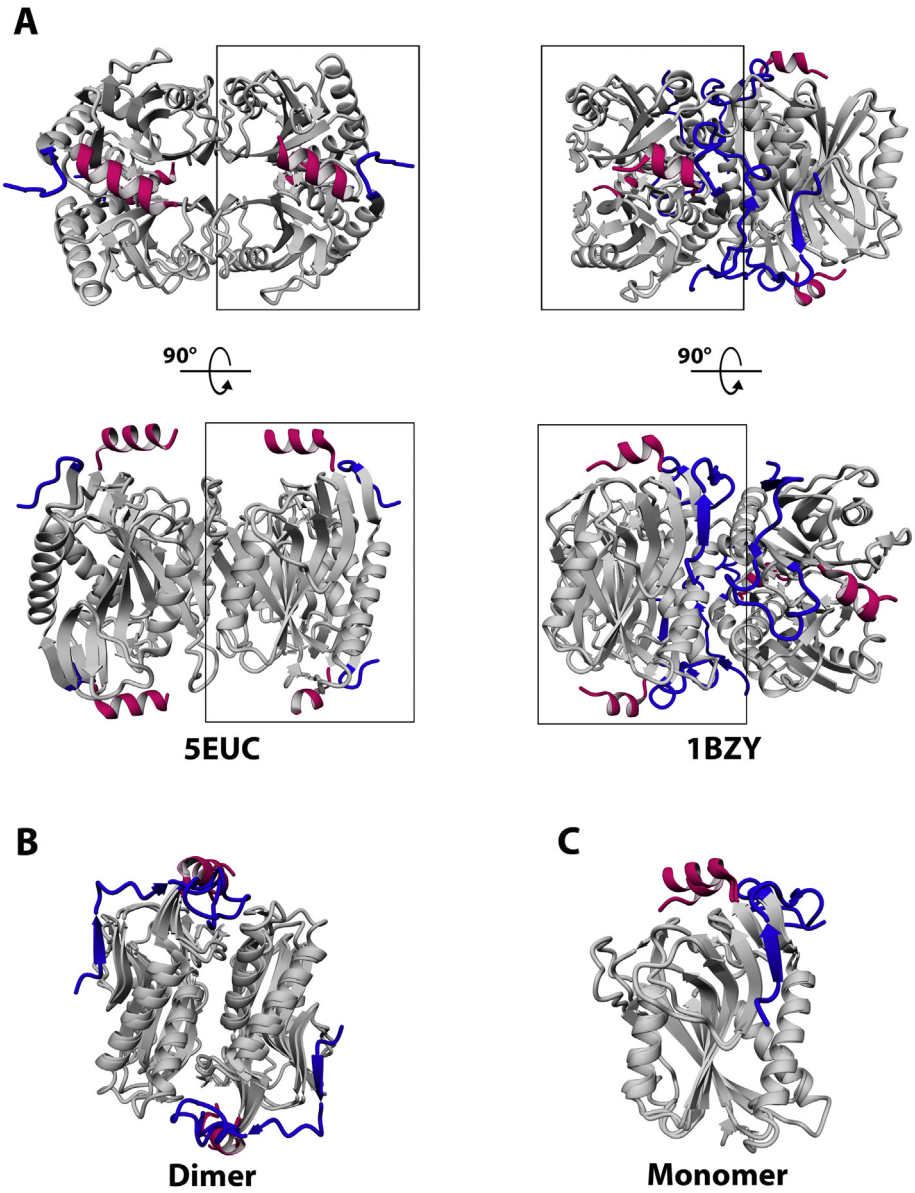

Fig. 12. Comparison between human HPRT (PDB ID: 1BZY) and TcHPRT (PDB ID: 5EUC). (A) Two orthogonal views of each structure are shown: 5EUC on the left and 1BZY on the right. The N- and C-terminal regions referred to in the main text are painted in blue and red, respectively. To stress the difference between the two tetrameric arrangements, the dimeric sets in the boxes are shown in the same pose. Indeed, they result from a rigid superimposition followed by horizontal translation apart from each other. Superimposition of dimers (B) and monomers (C) extracted from each structure.

whereas in the latter the N-terminal moieties participate in the interaction surface between dimers, in TcHPRT all N-termini point outwards. Nevertheless, a common dimeric interface in both tetrameric arrangements is conserved. This result emerges as strong evidence in favor of dimer 1 as the prevailing structure found in solution after proteolysis of full-length TcHPRT.

3.7. General conclusion

The influence of oligomeric structure on protein conformation pervades protein science. In this context, intriguing is the fact that regions that appear disordered exert key influence on the quaternary arrangement and play a modulatory role on enzymatic activity. This paper advances this knowledge in the case of TcHPRT, a critical enzyme for the survival of the parasite. Bisphosphonates act as pyrophosphate-mimetic inhibitors in this system, allowing the interrogation of the role of long-range influences on enzymatic activity.

Author contribution statement

WMV, planned and performed the experiments and analyzed the data; AC-S, performed the experiments and analyzed the data; LD, performed the simulations and analyzed the data; AM, performed the experiments and analyzed the data; AP, analyzed the data; JS, planned the experiments, analyzed the data and wrote the paper; JMD, planned the experiments, analyzed the data and wrote the paper.

Transparency Document

The Transparency document associated with this article can be found, in the online version.

Acknowledgments

We especially thank the IGBMC Structural genomics platform staff (in particular Pierre Poussin Courmontagne and Dr. Alastair McEwen). We thank Dr. Eduardo Howard for his fruitful comments regarding crystallization experiments. The crystallographic experiments were performed on the X06DA beamline at the Swiss Light Source, Paul Scherrer Institut, Villigen, Switzerland. In particular we thank Dr. Vincent Olieric for his help on the beamline. This work was funded by the National Center for Scientific Research (CNRS), the Institut National de la Santé et de la Recherche Médicale (INSERM), the Université de Strasbourg, the Région Alsace, the Hôpital Civil de Strasbourg, Instruct (part of the European Strategy Forum of Research Infrastructures; ESFRI), the French Infrastructure for Integrated Structural Biology (FRISBI) (ANR-10-INSB-05-01). This work was supported by the *Agencia Nacional de Promoción Científica y Tecnológica* (ANPCyT) (PICT 2011-0861), the *Consejo Nacional de Investigaciones Científicas y Técnicas* (CONICET) (PIP 1936) and the *Universidad de Buenos Aires* (UBACyT) (20020130100468BA).

Appendix A. Supplementary data

Supplementary data to this article can be found online at http://dx.doi.org/10.1016/j.bbapap.2016.03.005.

References

[1] R.L. Berens, J.J. Marr, S.W. LaFon, D.J. Nelson, Purine metabolism in *Trypanosoma cruzi*, Mol. Biochem. Parasitol. 3 (1981) 187–196.
[2] F. Sanchez-Sancho, N.E. Campillo, J.A. Paez, Chagas disease: progress and new perspectives, Curr. Med. Chem. 17 (2010) 423–452.
[3] M.N. Soeiro, S.L. de Castro, *Trypanosoma cruzi* targets for new chemotherapeutic approaches, Expert Opin. Ther. Targets 13 (2009) 105–121.
[4] M. Fasullo, L. Endres, Nucleotide salvage deficiencies, DNA damage and neurodegeneration, Int. J. Mol. Sci. 16 (2015) 9431–9449.
[5] K.V. Nguyen, W.L. Nyhan, Lesch–Nyhan syndrome in a family with a deletion followed by an insertion within the HPRT1 gene, Nucleosides Nucleotides Nucleic Acids 34 (2015) 442–447.
[6] M.W. Partington, B.K. Hennen, The Lesch–Nyhan syndrome: self-destructive biting, mental retardation, neurological disorder and hyperuricaemia, Dev. Med. Child Neurol. 9 (1967) 563–572.
[7] R.J. Torres, J.G. Puig, Hypoxanthine-guanine phosophoribosyltransferase (HPRT) deficiency: Lesch–Nyhan syndrome, Orphanet J. Rare Dis. 2 (2007) 48.
[8] D.G. Sculley, P.A. Dawson, B.T. Emmerson, R.B. Gordon, A review of the molecular basis of hypoxanthine-guanine phosphoribosyltransferase (HPRT) deficiency, Hum. Genet. 90 (1992) 195–207.
[9] G.K. Balendiran, J.A. Molina, Y. Xu, J. Torres-Martinez, R. Stevens, P.J. Focia, A.E. Eakin, J.C. Sacchettini, S.P. Craig 3rd, Ternary complex structure of human HGPRTase, PRPP, Mg^{2+}, and the inhibitor HPP reveals the involvement of the flexible loop in substrate binding, Protein Sci. 8 (1999) 1023–1031.
[10] B. Canyuk, P.J. Focia, A.E. Eakin, The role for an invariant aspartic acid in hypoxanthine phosphoribosyltransferases is examined using saturation mutagenesis, functional analysis, and X-ray crystallography, Biochemistry 40 (2001) 2754–2765.
[11] P.J. Focia, S.P. Craig 3rd, A.E. Eakin, Approaching the transition state in the crystal structure of a phosphoribosyltransferase, Biochemistry 37 (1998) 17120–17127.
[12] P.J. Focia, S.P. Craig 3rd, R. Nieves-Alicea, R.J. Fletterick, A.E. Eakin, A 1.4 A crystal structure for the hypoxanthine phosphoribosyltransferase of *Trypanosoma cruzi*, Biochemistry 37 (1998) 15066–15075.
[13] R. Nieves-Alicea, P.J. Focia, S.P. Craig 3rd, A.E. Eakin, Limited proteolysis of a trypanosomal hypoxanthine phosphoribosyltransferase yields crystals that diffract X-rays to near atomic resolution, Biochim. Biophys. Acta 1388 (1998) 500–505.
[14] B. Canyuk, F.J. Medrano, M.A. Wenck, P.J. Focia, A.E. Eakin, S.P. Craig 3rd, Interactions at the dimer interface influence the relative efficiencies for purine nucleotide synthesis and pyrophosphorolysis in a phosphoribosyltransferase, J. Mol. Biol. 335 (2004) 905–921.
[15] T.E. Allen, B. Ullman, Molecular characterization and overexpression of the hypoxanthine-guanine phosphoribosyltransferase gene from *Trypanosoma cruzi*, Mol. Biochem. Parasitol. 65 (1994) 233–245.
[16] A. Heroux, E.L. White, L.J. Ross, D.W. Borhani, Crystal structures of the *Toxoplasma gondii* hypoxanthine-guanine phosphoribosyltransferase-GMP and -IMP complexes: comparison of purine binding interactions with the XMP complex, Biochemistry 38 (1999) 14485–14494.
[17] D.T. Keough, A.L. Ng, D.J. Winzor, B.T. Emmerson, J. de Jersey, Purification and characterization of *Plasmodium falciparum* hypoxanthine-guanine-xanthine phosphoribosyltransferase and comparison with the human enzyme, Mol. Biochem. Parasitol. 98 (1999) 29–41.
[18] P.S. Monzani, J.D. Alfonzo, L. Simpson, G. Oliva, O.H. Thiemann, Cloning, characterization and preliminary crystallographic analysis of *Leishmania* hypoxanthine-guanine phosphoribosyltransferase, Biochim. Biophys. Acta 1598 (2002) 3–9.
[19] P.S. Monzani, S. Trapani, O.H. Thiemann, G. Oliva, Crystal structure of *Leishmania tarentolae* hypoxanthine-guanine phosphoribosyltransferase, BMC Struct. Biol. 7 (2007) 59.
[20] M.D. Winn, C.C. Ballard, K.D. Cowtan, E.J. Dodson, P. Emsley, P.R. Evans, R.M. Keegan, E.B. Krissinel, A.G. Leslie, A. McCoy, S.J. McNicholas, G.N. Murshudov, N.S. Pannu, E.A. Potterton, H.R. Powell, R.J. Read, A. Vagin, K.S. Wilson, Overview of the CCP4 suite and current developments, Acta Crystallogr. D Biol. Crystallogr. 67 (2011) 235–242.
[21] P. Emsley, K. Cowtan, Coot: model-building tools for molecular graphics, Acta Crystallogr. D Biol. Crystallogr. 60 (2004) 2126–2132.
[22] G.N. Murshudov, P. Skubak, A.A. Lebedev, N.S. Pannu, R.A. Steiner, R.A. Nicholls, M.D. Winn, F. Long, A.A. Vagin, REFMAC5 for the refinement of macromolecular crystal structures, Acta Crystallogr. D Biol. Crystallogr. 67 (2011) 355–367.
[23] L.M. Curto, J.J. Caramelo, J.M. Delfino, Delta98delta, a functional all-beta-sheet abridged form of intestinal fatty acid binding protein, Biochemistry 44 (2005) 13847–13857.
[24] S.E. Faraj, L. Venturutti, E.A. Roman, C.B. Marino-Buslje, A. Mignone, S.C. Tosatto, J.M. Delfino, J. Santos, The role of the N-terminal tail for the oligomerization, folding and stability of human frataxin, FEBS Open Bio 3 (2013) 310–320.
[25] M.E. Noguera, M.E. Primo, L.N. Sosa, V.A. Risso, E. Poskus, M.R. Ermacora, Biophysical characterization of the membrane-proximal ectodomain of the receptor-type protein-tyrosine phosphatase phogrin, Protein Pept. Lett. 20 (2013) 1009–1017.
[26] C.C. Lee, F.J. Medrano, S.P. Craig 3rd, A.E. Eakin, Investigation of the functional role of active site loop II in a hypoxanthine phosphoribosyltransferase, Biochim. Biophys. Acta 1537 (2001) 63–70.
[27] D. Fernandez, M.A. Wenck, S.P. Craig 3rd, J.M. Delfino, The purine transferase from *Trypanosoma cruzi* as a potential target for bisphosphonate-based chemotherapeutic compounds, Bioorg. Med. Chem. Lett. 14 (2004) 4501–4504.
[28] G. Neuberger, S. Maurer-Stroh, B. Eisenhaber, A. Hartig, F. Eisenhaber, Motif refinement of the peroxisomal targeting signal 1 and evaluation of taxon-specific differences, J. Mol. Biol. 328 (2003) 567–579.
[29] T. Hausler, Y.D. Stierhof, E. Wirtz, C. Clayton, Import of a DHFR hybrid protein into glycosomes in vivo is not inhibited by the folate-analogue aminopterin, J. Cell Biol. 132 (1996) 311–324.
[30] J.A. McNew, J.M. Goodman, An oligomeric protein is imported into peroxisomes in vivo, J. Cell Biol. 127 (1994) 1245–1257.
[31] F.J. Medrano, M.A. Wenck, A.E. Eakin, S.P. Craig 3rd, Functional roles for amino acids in active site loop II of a hypoxanthine phosphoribosyltransferase, Biochim. Biophys. Acta 1650 (2003) 105–116.
[32] D.A. Scott, W. de Souza, M. Benchimol, L. Zhong, H.G. Lu, S.N. Moreno, R. Docampo, Presence of a plant-like proton-pumping pyrophosphatase in acidocalcisomes of *Trypanosoma cruzi*, J. Biol. Chem. 273 (1998) 22151–22158.

[33] A. Montalvetti, B.N. Bailey, M.B. Martin, G.W. Severin, E. Oldfield, R. Docampo, Bisphosphonates are potent inhibitors of *Trypanosoma cruzi* farnesyl pyrophosphate synthase, J. Biol. Chem. 276 (2001) 33930–33937.
[34] S.H. Szajnman, A. Montalvetti, Y. Wang, R. Docampo, J.B. Rodriguez, Bisphosphonates derived from fatty acids are potent inhibitors of *Trypanosoma cruzi* farnesyl pyrophosphate synthase, Bioorg. Med. Chem. Lett. 13 (2003) 3231–3235.
[35] J.A. Urbina, B. Moreno, S. Vierkotter, E. Oldfield, G. Payares, C. Sanoja, B.N. Bailey, W. Yan, D.A. Scott, S.N. Moreno, R. Docampo, *Trypanosoma cruzi* contains major pyrophosphate stores, and its growth in vitro and in vivo is blocked by pyrophosphate analogs, J. Biol. Chem. 274 (1999) 33609–33615.
[36] T. Ishida, K. Kinoshita, PrDOS: prediction of disordered protein regions from amino acid sequence, Nucleic Acids Res. 35 (2007) W460–W464.
[37] R. Linding, L.J. Jensen, F. Diella, P. Bork, T.J. Gibson, R.B. Russell, Protein disorder prediction: implications for structural proteomics, Structure 11 (2003) 1453–1459.
[38] K. Shimizu, POODLE: tools predicting intrinsically disordered regions of amino acid sequence, Methods Mol. Biol. 1137 (2014) 131–145.
[39] M. Sickmeier, J.A. Hamilton, T. LeGall, V. Vacic, M.S. Cortese, A. Tantos, B. Szabo, P. Tompa, J. Chen, V.N. Uversky, Z. Obradovic, A.K. Dunker, DisProt: the database of disordered proteins, Nucleic Acids Res. 35 (2007) D786–D793.
[40] Z. Dosztanyi, V. Csizmok, P. Tompa, I. Simon, IUPred: web server for the prediction of intrinsically unstructured regions of proteins based on estimated energy content, Bioinformatics 21 (2005) 3433–3434.
[41] L. Whitmore, B.A. Wallace, DICHROWEB, an online server for protein secondary structure analyses from circular dichroism spectroscopic data, Nucleic Acids Res. 32 (2004) W668–W673.
[42] W. Kabsch, C. Sander, Dictionary of protein secondary structure: pattern recognition of hydrogen-bonded and geometrical features, Biopolymers 22 (1983) 2577–2637.